

An Overview of Energy-Optimal Impedance Control of Cooperative Robot Manipulators

Amin Ghorbanpour, Hanz Richter

Abstract—An impedance-based control scheme is introduced for cooperative manipulators grasping a rigid load. The position and orientation of the load are to be maintained close to a desired trajectory, trading off tracking accuracy by low energy consumption and maintaining stability. To this end, the augmented dynamics of the robots, their actuators and the load is formed, and an impedance control is adopted. A virtual control strategy is used to decouple torque control from actuator control. An optimization problem is then formulated using energy balance equations. The optimization finds the damping and stiffness gains of the impedance relation such that the energy consumption is minimized. Furthermore, \mathcal{L}_2 stability techniques are used to allow for time-varying damping and stiffness in the desired impedance. A numerical example is provided to demonstrate the results.

I. INTRODUCTION

SAVING energy has become a major driving force in engineering, owing to increasing demand for cost-efficient and long-life systems, and as a result, engineers sought to find solutions for optimal energy consumption. This is particularly important in robotic automation. Robots with on-board, finite energy storage are prevalent in electric vehicles, powered human assistive devices, aerospace vehicles, etc. [1], [2], [3], [4], [5], [6], [7], [8], [9], [10], [11].

Therefore, in dynamical systems with limited on-board energy source, longer operating times and smaller operating costs are possible by reducing the amount of energy needed to complete the motion tasks. Energy regeneration is defined here as the ability to transfer energy back to the system's power source during motion tasks. Energy-aware control in robotics, particularly concerning energy regeneration, has gained a broad research interest recently [1], [2], [8], [9], [6]. Ultracapacitors have been used in addition to or instead of batteries as energy storage elements in regenerative motion systems. In addition to being lightweight and durable, ultracapacitors can be charged and discharged at high rates. This feature is essential for energy regeneration because the storage element should be capable of admitting all the energy that can be potentially recovered.

So far, most studies have considered energy-oriented control in single robots where significant potential for energy recovery exists, e.g. industrial robots, prosthetic legs, etc. [7], [1], [6]. These works sought to minimize energy consumption by

maximizing regenerative energy storage relative to trajectories, controller parameters or design parameters. The latter problem was quadratic, and admitted explicit solutions.

The focus of this study is to introduce a framework for energy-oriented control in cooperative robots. Even though robots offer superior capabilities than humans for carrying out motion tasks involving large loads, speeds and tight precision requirements, some tasks are difficult or impossible for a single robot. The limits in the structure of a robot prevent a sole robot to operate with large, unbalanced or flexible loads. Cooperative robot manipulators (CRM) offer significant advantages over a single robot, and they show better performance in tasks such as grasping, gripping, lifting, transferring, lowering, and approach an object. Regardless of the benefits obtained by employing CRM, it comes at the cost of complexity for the mathematical modeling, control, and coordination. Here, the term cooperative means collaboration of multi robots in handling a payload.

This paper considers theoretical developments and extensions of a framework previously established for a single robot in [2]. Here, a motion task is defined as carrying a payload near a desired trajectory by grasping it using the CRM, limiting grasping forces and reducing energy consumption. The motion task thus demands a controller meeting three main objectives: 1) maintaining acceptable tracking accuracy of desired trajectories for the position and orientation of the load, 2) being in compliance with the closed kinematic chain caused by grasping the load, and 3) minimizing the energy consumption through energy regeneration. A novel controller is proposed based on an impedance relation whose parameters are tuned such that maximum energy regeneration is provided. It is assumed that all robots and their corresponding actuators (DC motors) are equipped with regenerative drives (4-quadrant drives), allowing energy to go back from the robots to the storage element. Regenerative drives provide an opportunity to harvest the excess mechanical energy by channeling it back to the source instead of being dissipated [1].

A. Review of related work

Most of the research literature on CRM does not place emphasis on energy considerations. Optimization of the energy consumption for single robots and general electromechanical systems is well documented [5], [2], [7], [1], [11], [4], [6], [3], [12], [13], [14], [15], [16]. In the field of robotics, researches in [2], [1], [4], [3] minimized energy consumption considering capacitive storage elements. These ideas were applied for powered human assistive devices [6], [11], [12], and aerospace

The authors are with the Department of Mechanical Engineering, Cleveland State University, Cleveland, OH 44122 USA (e-mail: a.ghorbanpour@csuohio.edu; h.richter@csuohio.edu).

This article is intended as a supplement to article titled "Energy-Optimal Impedance Control of Cooperative Robot Manipulators" written by the same authors.

applications [7], [14], [5]. Energy-oriented control studies have also been conducted with a focus on actuator design and dynamics [3], [15], [16].

The framework established in [2] combines the dynamics of a robot, joint mechanisms, and actuators to present an augmented dynamical model of the robotic system. Depending on the type of the actuators, e.g. DC motors, hydraulic elements, etc., the energy transfer between the power source and the actuators can be derived, which leads to find the energy change in the power source. Hence, an energy minimization can be formed. These ideas were applied to an industrial robot (PUMA manipulator), finding point-to-point energy-optimal trajectories [1]. It is shown that 10-20% energy reduction is possible by energy regeneration. Furthermore, application of the idea for prosthetic leg showed promising results [6], [17], [12].

In the aforementioned works, robots are either isolated without any contact with the environment, or have limited (in the sense of low and intermittent interaction forces) interactions with it. Accordingly, interactions were not modeled and regarded as external disturbances. This work provides a bridge between energy-oriented control works and the subject of cooperative robots, considering the stability of interactions.

Modeling and control of CRM have received wide attention for more than 3 decades [18], [19], [20], [21], [22], [23], [24], [25], [26], [27], [28], [29], [30], [31], [32], [33], [34], [35], [36]. Nevertheless, the energy-oriented studies of CRM have received little attention. For instance, in [23] energy consumption is reduced by finding the optimal operating schedule of a robotic manufacturing system, using the consumption profiles of individual robots and their operations as pre-determined information.

CRM tasks involve interaction between the robots and a payload, and the force-position relationships between them are of fundamental concern. For trajectory tracking, various control approaches have been proposed, with impedance control being prevalent. Impedance control constitutes an effective, easy-to-implement scheme for multiple interacting dynamical systems. Impedance control includes regulation and stabilization of robot motion by establishing a mathematical relationship between the interaction forces/moments and the robot trajectories. The relation usually defined as a second order linear non-homogeneous ordinary differential equation, often modeled after a forced spring-mass-damper system. Impedance control has been used for CRM in many works, for instance [26], [34], [25], [27], [32], [33], [29], [35], [36], [30], [31], [28].

One of the main differences among various approaches is the definition of terms and the structure of the impedance relationship. This includes different choices of the forces or moments appearing in the impedance relation [26], [25] or the use of nonlinear [28] and variable [29] inertial, stiffness and damping characteristics.

Furthermore, impedance control is useful when the payload handled by the CRM may also be in contact with the environment. The algorithm of [30] controls motion and internal forces of the payload, as well as the contact forces between the payload and environment. In that work, the reference trajectory

for each robotic joint is calculated based on an impedance relationship such that the desired internal and contact forces are achieved. In [31] the problem of assembly operations using CRM was considered. Experiments showed the effectiveness of impedance controls for typical tasks encountered in CRM systems.

Impedance relationships have also been used in conjunction with adaptive control, as an alternative to reduce the system's sensitivity due to modeling mismatch. In [32], an adaptive strategy is used to generate a desired motion trajectory in compliance with desired forces at the end effectors, even when the payload stiffness is unknown. Furthermore, adaptation is used in [33] to obtain variable damping and stiffness, exhibiting different impedance characteristics according to the forces exerted by the environment.

In this paper, passivity techniques are used to guarantee system stability in the presence of interaction forces and moments between the payload and the robots.

The remainder of the paper is organized as follows: In Section II, mathematical preliminaries and a brief background on passivity and \mathcal{L}_2 stability results are presented. In Section III, a model of the CRM is presented. Section IV discusses the semi-active control implementation and associated energy balance equations. The overall control architecture and the impedance control approach are discussed in sections V and VI, respectively. Section VII introduces the optimization and a numerical simulation is presented in section VIII. Finally, conclusions and recommendations for future work are given in section IX.

II. MATHEMATICAL PRELIMINARIES

In this section, we briefly recall some basic properties and classical results of input-output stability and passive systems [37], [38]. Denote \mathbb{R}_+ as the set of non-negative real numbers, and let \mathbb{R}^n be the n -dimensional vector space over \mathbb{R} . Define Π as the set of all measurable, real-valued, n -dimensional functions of time $f(t) : \mathbb{R}_+ \rightarrow \mathbb{R}^n$ and $t \in \mathbb{R}_+$ and define the sets:

$$\mathcal{L}_2^n \triangleq \{x \in \Pi \mid \|f\|_2^2 \triangleq \int_0^\infty \|f(t)\|^2 dt < \infty\} \quad (1a)$$

$$\mathcal{L}_\infty^n \triangleq \{x \in \Pi \mid \|f\|_\infty^2 \triangleq \sup_t \|f(t)\|^2 < \infty\} \quad (1b)$$

with $\|\cdot\|$ the standard Euclidean norm. Also, extended spaces are defined as:

$$\mathcal{L}_{2e}^n \triangleq \{x \in \Pi \mid \|f\|_{2,T}^2 \triangleq \int_0^T \|f(\xi)\|^2 d\xi < \infty, \forall T \in \mathbb{R}_+\} \quad (2a)$$

$$\mathcal{L}_{\infty e}^n \triangleq \{x \in \Pi \mid \|f\|_{\infty,T}^2 \triangleq \sup_T \|f(T)\|^2 < \infty, \forall T \in \mathbb{R}_+\} \quad (2b)$$

Here, \mathcal{L}_2^n and \mathcal{L}_{2e}^n are inner product spaces. The truncated inner product of two functions $u(t), y(t) \in \mathcal{L}_{2e}^n$ is defined as:

$$\langle y|u \rangle_T \triangleq \int_0^T u^T(\xi)y(\xi)d\xi \quad (3)$$

where the two functions can be related by a dynamical operator, H , such that $y = H(u)$. The operator H is called

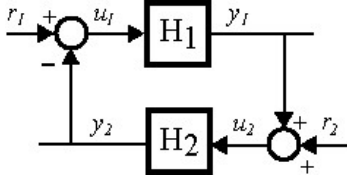


Fig. 1. Feedback interconnection with two external inputs.

causal if the value of output, y , at time t is a function of the value of input, u , up to time t [38]. For a causal operator, we have the following definitions:

Definition 1. Let $H : \mathcal{L}_{2e}^n \rightarrow \mathcal{L}_{2e}^n$ be a causal dynamic operator and $y = H(u)$ is the output. Then for some non-negative constants β , ϵ and δ , and $\forall u \in \mathcal{L}_{2e}^n$, $H(\cdot)$ is called input-output strict passive (IOSP) if:

$$\langle y|u \rangle_T \geq \epsilon \|u\|_{2,T}^2 + \delta \|y\|_{2,T}^2 - \beta \quad (4)$$

H is called passive if $\epsilon = \delta = 0$, output strictly passive (OSP) if $\epsilon = 0$, and input strictly passive (ISP) if $\delta = 0$ [38].

Definition 2. The causal dynamical operator $H : \mathcal{L}_{2e}^n \rightarrow \mathcal{L}_{2e}^n$ is said to be finite-gain \mathcal{L}_2 stable if there are non-negative constants γ_0 and β_0 such that [39], [38]:

$$\|y\|_{2,T} \leq \gamma_0 \|u\|_{2,T} + \beta_0 \quad \forall T \geq 0 \quad (5)$$

So far, we have defined the concept of input-output stability for a single causal system. The results can be extended for the feedback system as shown in Fig. 1. Here we assume the feedback interconnection is well-defined. That is for $r \triangleq (r_1, r_2)$ and $y \triangleq (y_1, y_2)$, the mapping $y = \tilde{H}(r)$ is causal and $\tilde{H} : \mathcal{L}_{2e}^n \rightarrow \mathcal{L}_{2e}^n$.

We elaborate the following result for the feedback interconnection:

Lemma 1. Consider the well-defined feedback interconnection of two IOSP causal operator dynamical systems H_1 and H_2 as shown in Fig. 1. The following inequality is effective:

$$c_1 \|y_1\|_{2,T}^2 + c_2 \|y_2\|_{2,T}^2 \leq c_3 \|r_1\|_{2,T}^2 + c_4 \|r_2\|_{2,T}^2 - \hat{\beta} \quad (6)$$

where:

$$\begin{aligned} c_1 &= \{(\delta_1 + \epsilon_2) - \frac{\gamma_1}{2} - \epsilon_2 \gamma_4\} \\ c_2 &= \{(\delta_2 + \epsilon_1) - \frac{\gamma_2}{2} - \epsilon_1 \gamma_3\} \\ c_3 &= \left\{ \frac{1}{2\gamma_1} + \frac{\epsilon_1}{\gamma_3} \right\} \\ c_4 &= \left\{ \frac{1}{2\gamma_2} + \frac{\epsilon_2}{\gamma_4} \right\} \end{aligned}$$

for $\gamma_j > 0, j \in \{1, 2, 3, 4\}$ and constant $\hat{\beta} > 0$.

Proof. Since H_1 and H_2 are IOSP, we have:

$$\langle y_i|u_i \rangle_T \geq \epsilon_i \|u_i\|_{2,T}^2 + \delta_i \|y_i\|_{2,T}^2 - \beta_i \quad i \in \{1, 2\} \quad (7)$$

From Fig. 1, we have $u_1 = r_1 - y_2$ and $u_2 = r_2 + y_1$, therefore:

$$\langle y_1|u_1 \rangle_T + \langle y_2|u_2 \rangle_T = \langle y_1|r_1 \rangle_T + \langle y_2|r_2 \rangle_T \quad (8)$$

Using the interconnection relations, we can write:

$$\begin{aligned} \|u_1\|_{2,T}^2 &= \|r_1\|_{2,T}^2 + \|y_2\|_{2,T}^2 - 2\langle y_2|r_1 \rangle_T \\ &\geq \|y_2\|_{2,T}^2 - 2\langle y_2|r_1 \rangle_T \end{aligned} \quad (9a)$$

$$\begin{aligned} \|u_2\|_{2,T}^2 &= \|r_2\|_{2,T}^2 + \|y_1\|_{2,T}^2 + 2\langle y_1|r_2 \rangle_T \\ &\geq \|y_1\|_{2,T}^2 + 2\langle y_1|r_2 \rangle_T \end{aligned} \quad (9b)$$

Using equations (7), (8), and (9), we have the following inequality:

$$\begin{aligned} \langle y_1|r_1 \rangle_T + \langle y_2|r_2 \rangle_T + 2\epsilon_1 \langle y_2|r_1 \rangle_T - 2\epsilon_2 \langle y_1|r_2 \rangle_T \geq \\ (\delta_1 + \epsilon_2) \|y_1\|_{2,T}^2 + (\delta_2 + \epsilon_1) \|y_2\|_{2,T}^2 - \beta_1 - \beta_2 \end{aligned} \quad (10)$$

Using the Cauchy-Schwarz inequality, for any two arbitrary signals r and y , there is a $\gamma > 0$, such that:

$$\begin{aligned} \langle y|r \rangle_T &\leq \|y\|_{2,T} \|r\|_{2,T} + \frac{1}{2} \left(\frac{1}{\sqrt{\gamma}} \|r\|_{2,T} - \sqrt{\gamma} \|y\|_{2,T} \right)^2 \\ &\leq \frac{1}{2\gamma} \|r\|_{2,T}^2 + \frac{\gamma}{2} \|y\|_{2,T}^2 \end{aligned} \quad (11a)$$

$$\begin{aligned} \langle y|r \rangle_T &\geq -\|y\|_{2,T} \|r\|_{2,T} - \frac{1}{2} \left(\frac{1}{\sqrt{\gamma}} \|r\|_{2,T} - \sqrt{\gamma} \|y\|_{2,T} \right)^2 \\ &\geq -\frac{1}{2\gamma} \|r\|_{2,T}^2 - \frac{\gamma}{2} \|y\|_{2,T}^2 \end{aligned} \quad (11b)$$

If we assign $\gamma_1, \gamma_2, \gamma_3$ as constants for the pair of signals (r_1, y_1) , (r_2, y_2) , and (r_1, y_2) , respectively, in inequality (11a), and γ_4 for (r_2, y_1) in inequality (11b), then by substituting the obtained inequalities in inequality (10) and with some simplification and manipulation, equation (6) can be obtained. \square

Finally, we list two useful standard results:

Lemma 2. The feedback in Fig. 1 is finite-gain \mathcal{L}_2 stable if $\delta_1 + \epsilon_2 > 0$, $\delta_2 + \epsilon_1 > 0$ [40].

Theorem 1. Let $y = H(s)u$, where $H(s) \in \mathbb{R}^{n \times n}$ is an exponentially stable and strictly proper transfer function. If $u \in \mathcal{L}_2$, then $y \in \mathcal{L}_2 \cap \mathcal{L}_\infty$, $\dot{y} \in \mathcal{L}_2$ and $y \rightarrow 0$ as $t \rightarrow \infty$. In addition, if $u \rightarrow 0$ as $t \rightarrow \infty$, then $\dot{y} \rightarrow 0$ [38], [41].

III. MODELING

In this section, we introduce the dynamical model of N cooperative robots carrying a rigid load by grasping it as shown in Fig. 2. The objective in this section is to model the robots, the load and to establish the coupling between the robots. First we build the augmented model of each robot, its joint mechanisms and the DC motor actuators. Then, based on the augmented model of the individual robots, a comprehensive model of the cooperative robots is introduced. The load is modeled assuming to be a rigid object. Finally, the kinematic and dynamic coupling of the closed chain system is discussed.

To develop the dynamics equations, for the remainder of this paper, unless otherwise told, the following notations are used: any parameter with subscript i indicates the parameter for i th robot, $i \in \{1, \dots, N\}$, and subscript ij indicates the parameter for j th joint of i th robot, $j \in \{1, 2, \dots, n\}$.

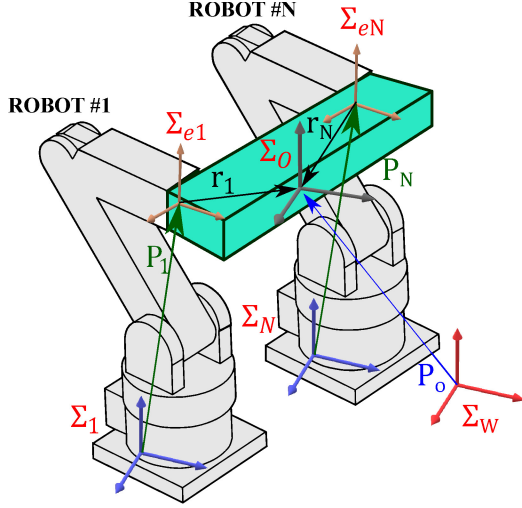


Fig. 2. Illustration of N robots grasping an object. The coordinate frames attached to the end-effector, robots' base, load's center of mass, and arbitrary world frame are, respectively, Σ_{ei} , Σ_i , Σ_o , Σ_w .

A. Comprehensive dynamics of cooperative robots

We assume there are N non-redundant robots carrying an object. The dynamics of i th robot, without considering the drive systems, modeled as:

$$D_i^o(q_i)\ddot{q}_i + C_i^o(q_i, \dot{q}_i)\dot{q}_i + g_i(q_i) = \tau_i + J_i^T(q_i)F_i \quad (12)$$

where $q_i \in \mathbb{R}^n$ is the vector of joint coordinates, $D_i^o(q_i)$ is the inertia matrix, $C_i^o(q_i)$ is the matrix accounting for centripetal and Coriolis effects, $g_i(q_i)$ is the gravity vector, $J_i \in \mathbb{R}^{n \times n}$ is the Jacobian matrix which is assumed to be nonsingular, $F_i = [f_i^T, m_i^T]^T \in \mathbb{R}^n$ is the vector of forces (f_i) and moments (m_i) applied by the object at the end-effector, and $\tau_i = [\tau_{i1}, \tau_{i2}, \dots, \tau_{in}]^T \in \mathbb{R}^n$ is the vector of forces/moments applied at the joints.

All n joints of the robot are considered to be *semi-active*. A semi-active joint mechanism (JM) only exchange mechanical power with the robot, and it is connected to an electric energy storage element source, e.g. an ultracapacitor. We consider that all semi-active joints of all robots are connected to a common storage element, as illustrated in Fig 3, and they are regenerative, allowing the power source to be charged whenever surplus mechanical energy from the robots is available to flow back through DC motors. Also, in each semi-active JM, the interface torque between the JM and the j th robot link can be described by:

$$\tau_{ij} = -J_{ij}\bar{n}_{ij}^2\ddot{q}_{ij} - b_{ij}\bar{n}_{ij}^2\dot{q}_{ij} + \bar{n}_{ij}\tau_{ind_{ij}} \quad (13)$$

where J_{ij} , \bar{n}_{ij} , and b_{ij} are the JM moment of inertia, the gear ratio, and friction coefficient, respectively. $\tau_{ind_{ij}} = \alpha_{ij}I_{ij}$ is the induced torque of the motor, where I_{ij} is the current in the motor and α_{ij} is the motor constant.

By combining the dynamics of robot and JMs, the augmented model of robot-JMs can be obtained. This can be done by finding $\tau_{ind_{ij}}$. In each JM, an ideal regenerative four-quadrant power conversion element (motor driver) is used to control the amount and direction of the applied voltage to

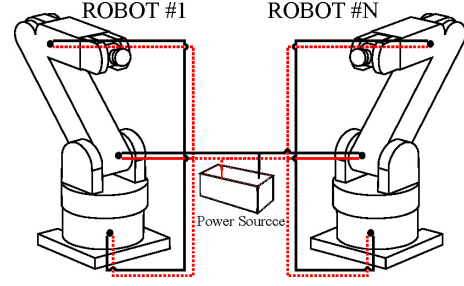


Fig. 3. Illustration of semi-active joints connection to a single power source.

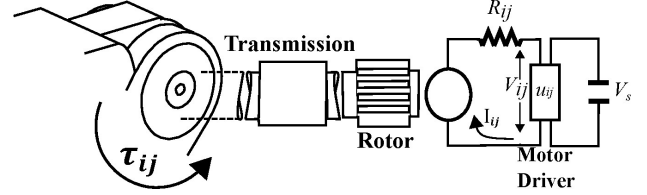


Fig. 4. Semi-active joint setup and its connection to motor driver and ultracapacitor.

the DC motor. Fig. 4 shows the model of the JM, where the converter voltage ratio is defined as $u_{ij} = V_{ij}/V_s$. With this, the applied voltage to a motor can be written as:

$$V_{ij} = R_{ij}I_{ij} + a_{ij}\dot{q}_{ij} \quad (14)$$

where R_{ij} is the resistance of the motor, and $a_{ij} = \alpha_{ij}\bar{n}_{ij}$ [1]. By substituting V_{ij} with u_{ij} in equation (14) and obtaining the induced torque of motor as a function of voltage ratio and angular velocity and finally, substituting the induced torque in equation (13), the applied torque can be rewritten as:

$$\tau_{ij} = -J_{ij}\bar{n}_{ij}^2\ddot{q}_{ij} - (b_{ij}\bar{n}_{ij}^2 + \frac{a_{ij}^2}{R_{ij}})\dot{q}_{ij} + \frac{a_{ij}u_{ij}}{R_{ij}}V_s \quad (15)$$

Replacing τ_{ij} from equation (15) into equation (12) and moving terms containing \dot{q}_i and \ddot{q}_i from right- to left-hand side, yields the following augmented robot-JM model:

$$D_i(q_i)\ddot{q}_i + C_i(q_i, \dot{q}_i)\dot{q}_i + g_i(q_i) = \mathcal{T}_i + J_i^T(q_i)f_i \quad (16)$$

where in the coupled dynamics, D_i^o and D_i are the same in all elements except in diagonal elements such that: $D_i = D_i^o + \text{diag}(J_{ij}\bar{n}_{ij}^2)$, also C_i and C_i^o are only different in diagonal terms such that $C_i = C_i^o + \text{diag}(b_{ij}\bar{n}_{ij}^2 + a_{ij}^2/R_{ij})$, and $\mathcal{T}_i = [U_{i1}, \dots, U_{in}]^T$, where:

$$U_{ij} = \frac{a_{ij}u_{ij}}{R_{ij}}V_s \quad (17)$$

Finally, by combining the augmented dynamics of all N robots, the comprehensive dynamics of CRM can be written as:

$$D(q)\ddot{q} + C(q, \dot{q})\dot{q} + G(q) = \mathcal{T} + J^T(q)F \quad (18)$$

where $X = [X_1^T, \dots, X_N^T]^T$, $X \in \{q, G, \mathcal{T}, F\}$ and $Y = \text{diag}(Y_1, \dots, Y_N)$, $Y \in \{D, C, J\}$. Hereafter, for ease of notation, we use $J^T(q)F \triangleq \mathcal{T}_{ext}$.

B. Dynamics of the load

The dynamics and kinematics of manipulators are coupled because the contact forces in all robots are interacting through the load. The dynamic coupling effects can be measured using the dynamics of the load. It is assumed that the mass of load is in its center of mass at Σ_O and the orientation is the orientation of coordinate frame Σ_O as shown in Fig. 2. In the world frame (Σ_W), the translation and rotation dynamics for the load are:

$$\begin{bmatrix} m_o I_{3 \times 3} & 0_{3 \times 3} \\ 0_{3 \times 3} & I_o \end{bmatrix} \begin{bmatrix} \ddot{P}_o \\ \dot{\omega}_o \end{bmatrix} + \begin{bmatrix} -m_o \mathbf{g} \\ \Omega_o I_o \omega_o \end{bmatrix} = J_o^T f \triangleq F_o \quad (19)$$

where $[P_o^T, \omega_o^T]^T = [x_o, y_o, z_o, \omega_x, \omega_y, \omega_z]^T$ is the vector of positions and angular velocities of the load. $I_{3 \times 3}$ and $0_{3 \times 3}$ are the identity and the null matrices, respectively, m_o is the mass of the load, and I_o is the moment of inertia about the center of mass. Ω_o is a skew-symmetric matrix, representing the cross product of $\omega_o \times I_o \omega_o$, F_o is the vector of all forces/moments applied at the center of mass of load, and $J_o^T = [J_{o1}^T \dots J_{oN}^T] \in \mathbb{R}^{6 \times 6N}$ is called the grasp matrix and defined as:

$$J_o^T = \begin{bmatrix} I_{3 \times 3} & 0_{3 \times 3} & \dots & I_{3 \times 3} & 0_{3 \times 3} \\ -S(r_1) & I_{3 \times 3} & \dots & -S(r_N) & I_{3 \times 3} \end{bmatrix} \quad (20)$$

where r_i is the vector from Σ_{ei} to Σ_o (see Fig. 2) and $S(r_i)$ is a skew-symmetric matrix, representing $r_i \times F_i$. The applied forces/moments by manipulators, f , can be decomposed to motion-inducing and internal parts as:

$$f = f_M + f_I \quad (21)$$

where f_M is the motion-inducing part that may balance the object's dynamics and f_I is the internal part consists of compressive, tensile and torsion forces/moments. Since f_I does not contribute to the motion of the object and has no net force, thus it spans the null space of J_o^T . Based on this fact, decomposition as equations (22) can be used to find f_M and f_I where $(J_o^T)^+$ is the generalized inverse of J_o^T [25].

$$f_M \triangleq [f_{M1}^T, \dots, f_{MN}^T]^T = (J_o^T)^+ J_o^T f \quad (22a)$$

$$f_I \triangleq [f_{I1}^T, \dots, f_{IN}^T]^T = (I_{6N \times 6N} - (J_o^T)^+ J_o^T) f \quad (22b)$$

Using equations (22) requires measuring force/moment at the end-effectors. This can be accomplished by installing a force sensor. To avoid direct measurement of force/moment, methods based on load distribution are introduced in [22], [20], [24]

C. Coupling in cooperative robots

The dynamics (load dynamics) and kinematics coupling cause constraint motion in each robot due to the closed chain configuration of the CRM. The kinematics coupling is defined as a set of equations, relating the translational and the rotational motions of the end-effectors that hold and move the rigid load securely [18]. In the world frame, the translational and rotational constraints are defined as:

$$P_i(q_i) + r_i(q_i) = P_j(q_j) + r_j(q_j) \quad (23a)$$

$$\Gamma_i(q_i) - \Gamma_k(q_k) = \delta R_{ii} \quad i, i \in \{1, \dots, N\} \quad (23b)$$

where the first constraint expresses the concatenated vectors, through each robot, that connect Σ_w to Σ_o , $\Gamma_i(q_i)$ is the vector that expresses the orientation of the i th end-effector, and δR_{ii} is a constant vector showing the difference between the orientation of the end-effectors at all time of the maneuver.

For N robots, there are $N(N-1)/2$ translational constraint vectors in the format of equation (23a) which each constraint contains three independent scalar equations, i.e. constraints in $(X, Y, Z)_W$ directions. There are $N(N-1)/2$ rotational constraint vectors in the format of equation (23b). Depending on the representation of the orientation, e.g. Euler or quaternion, various number of scalar constraints can be obtained.

IV. CONTROL IMPLEMENTATION AND ENERGY BALANCES

To devise a control scheme for CRM, there are two main consecutive steps. The first step is to design a controller to achieve the motion control objective of CRM; moving an object along a desired trajectory while grasping it securely without any damage to either object or robots. In the second step, a relationship is established between the control signal in the first step and the voltage ratios u_{ij} , which are available control inputs. This arises from the incorporation of storage element voltage feedback V_s in the augmented model. The voltage ratios u_{ij} are adjusted in this work using a method called semi-active virtual control (SVC) [2]. Using SVC enables us to describe energy exchange with the storage element and write energy balance equations for the closed system including robots and storage elements.

A. Semi-active virtual control strategy

Assume that a motion controller, called virtual control law (τ_{ij}^v), for U_{ij} in equation (18) has been designed. For τ_{ij}^v to meet the control objectives for the augmented model, a solution for u_{ij} is sought that enforces:

$$\tau_{ij}^v = \frac{a_{ij} u_{ij}}{R_{ij}} V_s \quad (24)$$

To design the virtual control, any feedback law compatible with the desired motion control objectives can be selected. If virtual matching, i.e. $\tau_{ij}^v = U_{ij}$, holds at all times, properties that apply to the virtual design such as stability, tracking performance, robustness, etc. will be propagated to the actual system. Virtual matching is possible as long as the storage element has nonzero voltage and it will hold exactly whenever the power converters are not saturated (e.g., $-1 \leq u_{ij} \leq 1$) and there is accurate knowledge of parameters a_{ij} and R_{ij} . The modulation law for exact virtual matching is obtained by solving for u_{ij} from equation (24).

The SVC technique uses V_s as feedback information in the virtual matching of equation (24). This approach permits the formulation of control laws and energy balance equations *without the need for a model of the storage element*. Devices such as ultracapacitors and batteries have complex and uncertain models.

B. Internal and external energy balance

The internal energy balance describes the power exchange between the semi-active joints and power storage element. Assuming there is no power lost during power exchange between the power source and DC motors, the input/output power balance for the motor drives can be written as:

$$V_s I_s = \sum_{i=1}^N \sum_{j=1}^n V_{ij} I_{ij} \quad (25)$$

where V_s and I_s are the voltage and current of the power storage, respectively. Dividing both sides by V_s , substituting current from equation (14) into equation (25), and taking the integral in the time interval $[0, T]$, the internal energy balance equation can be obtained as follows:

$$\Delta E_s = \int_0^T (\dot{q}^T \mathcal{T}^v - (\mathcal{T}^v)^T R_a \mathcal{T}^v) dt \quad (26)$$

where ΔE_s is the electric energy change in the power storage, $\mathcal{T}^v = [(\tau_1^v)^T, \dots, (\tau_N^v)^T]^T$, $\tau_i^v = [\tau_{i1}^v, \dots, \tau_{in}^v]^T$, and $R_a = \text{diag}(R_{ij}/a_{ij}^2) \in \mathbb{R}^{nN \times nN}$. The electric energy, E_s is assumed to be a positive-definite function of the power storage charge y , i.e. $E_s = E_s(y)$. We assume during a maneuver, there is enough charge in the storage element for maneuver execution. An example of a power source is the ultracapacitor. All results obtained in this section can be used interchangeably for virtual control design using an ultracapacitor as power source, i.e. $V_s \triangleq V_{cap}$.

An external energy balance for CRM can be derived as:

$$W_{ext} = \Delta E_c + \Delta E_m^{Tot} + \Sigma_m^{Tot} + \Sigma_e \quad (27)$$

where W_{ext} is the work done by external forces/moments, ΔE_m^{Tot} is the change in the mechanical energy of CRM, Σ_m^{Tot} is the mechanical losses, and Σ_e is the resistance heating (Joule) losses [1]. The derivation and definition of terms in equation (27) is outlined in Appendix A.

V. CONTROL SCHEME

In this study, the motion task is defined as following a desired trajectory closely but allowing deviations from the desired trajectory to limit the interaction forces/moments that could damage the robots or load. This can be captured by requiring all internal signals in a feedback control loop to be bounded, which is conveniently achieved with the passivity and \mathcal{L}_2 stability tools. Therefore, a control scheme based on impedance relation is developed to accomplish the motion task. Impedance control enforces a compliant behavior to avoid large values of contact force/moment [25], [34]. This technique is particularly useful in CRM since there is interaction between robots and the load.

The proposed control scheme is according to Fig (5). We assume the load's center of mass is following a pre-designed desired trajectory in world space. That is, the translational and rotational information of center of mass are P_o^d and R_o^d , respectively.

For the i th robot, the end-effector's desired position (P_i^d), orientation (R_{ei}^d), linear velocity (\dot{P}_i^d), angular velocity (ω_{ei}^d),

proportional linear acceleration (\ddot{P}_i^d), and angular acceleration ($\dot{\omega}_{ei}^d$) can be calculated using:

$$\begin{aligned} P_i^d &= P_o^d - R_o^d r_i \\ R_{ei}^d &= R_o^d \\ \dot{P}_i^d &= \dot{P}_o^d + S(R_o^d r_i) \omega_o^d \\ \omega_{ei}^d &= \omega_o^d \\ \ddot{P}_i^d &= \ddot{P}_o^d + S(\omega_o^d) S(R_o^d r_i) \omega_o^d + S(R_o^d r_i) \dot{\omega}_o^d \\ \dot{\omega}_{ei}^d &= \dot{\omega}_o^d \end{aligned} \quad (28)$$

where $S(\cdot)$ is the matrix performing cross-product and R_o^d is a matrix transformation that transfers r_i from object's frame (Σ_o) to the frame attached to the i th end-effector (Σ_{ei}) [34]. Using translational and rotational information of the end-effector, from Equation. (28), kinematics of the robot, and any inverse kinematics technique, the desired position (q_i^d), velocity (\dot{q}_i^d) and acceleration (\ddot{q}_i^d) of joints, can be obtained [42], [34]. The desired states in joint space along with the actual states and the interaction force between robots and the load are used in the impedance relation to calculate the virtual control, \mathcal{T}^v . The SVC uses the power source voltage information to regulate the virtual control and creates the actual control signal.

VI. IMPEDANCE CONTROL

The characteristics of an impedance control problem are given as a relationship between a desired trajectory and a desired dynamics. In this sense, the system is forced to establish a mathematical relationship between the interaction forces and the position error. To design the virtual control, we enforce the following relationship introduced in [41]:

$$\lim_{t \rightarrow \infty} M \ddot{\tilde{q}} + B \dot{\tilde{q}} + K \tilde{q} = \mathcal{T}_{ext} \quad (29)$$

where $\tilde{q} = q^d - q$ and the inertia (M), damping (K), and stiffness (K) are diagonal positive-definite matrices called gain matrices here, and all parameters are defined for each robot accordingly.

To achieve the objective in equation 29, we define an auxiliary error as:

$$\zeta = \tilde{q} - [p^2 M + pB + K]^{-1} \mathcal{T}_{ext} \quad (30)$$

where $p = d/dt$. It is easy to verify that if ζ converges to zero, the desired impedance in equation (29) is achieved. Therefore, we define the following variables:

$$S = -(\dot{\zeta} + \Lambda \zeta) \quad (31a)$$

$$\dot{q}_r = \dot{q} - S \quad (31b)$$

where Λ is a diagonal positive definite matrix. The virtual torque can be calculated using:

$$\mathcal{T}^v = D(q) \ddot{q}_r + C(q, \dot{q}) \dot{q}_r + G(q) - K_D S - \mathcal{T}_{ext} \quad (32)$$

where K_D is a positive definite matrix. From a practical point of view, \dot{q}_r and \ddot{q}_r in equation. (32) can be implemented by:

$$\dot{q}_r = \dot{q}^d + \Lambda \tilde{q} - (pI + \Lambda) [p^2 M + pB + K]^{-1} \mathcal{T}_{ext} \quad (33a)$$

$$\ddot{q}_r = \ddot{q}^d + \Lambda \dot{\tilde{q}} - p(pI + \Lambda) [p^2 M + pB + K]^{-1} \mathcal{T}_{ext} \quad (33b)$$

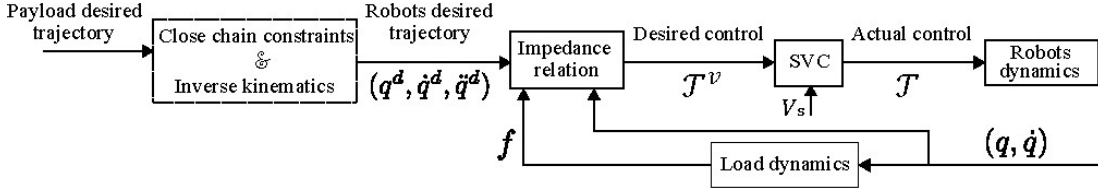


Fig. 5. Control scheme to control CRM in joint space, using impedance relation and SVC.

which shows that the implementation of the controller does not require the measurement of the acceleration.

Theorem 2. Consider the auxiliary error in equation (30) and S in equation (31a). Then the followings hold:

- (a) $S \in \mathcal{L}_2$
- (b) $\zeta \in \mathcal{L}_2 \cap \mathcal{L}_\infty$, $\dot{\zeta} \in \mathcal{L}_2$
- (c) $\zeta \rightarrow 0$ as $t \rightarrow \infty$.
- (d) $q, \dot{q} \in \mathcal{L}_{2e}$ and bounded.

and therefore, the closed-loop system is \mathcal{L}_2 finite gain stable.

Proof. (a) Assuming $\mathcal{T}^v = \mathcal{T}$, by substituting equation (32) in equation (18), the closed-loop system is obtained as:

$$D(q)\dot{S} + [C(q, \dot{q}) + K_D]S = 0 \quad (34)$$

We choose the following Lyapunov function candidate for the closed-loop system:

$$V(t) = \frac{1}{2} S^T D(q) S \quad (35)$$

Differentiating Lyapunov function with respect to time and with some manipulation and simplification, it yields:

$$\dot{V}(t) = -S^T K_D S \quad (36)$$

Equations (35) and (36) imply that S is asymptotically stable and therefore $S \in \mathcal{L}_2$.

(b,c) Using the definition of S in equation (31a), ζ and its derivative can be written as:

$$\zeta = -(pI + \Lambda)^{-1} S \quad (37a)$$

$$\dot{\zeta} = -p(pI + \Lambda)^{-1} S \quad (37b)$$

where $(pI + \Lambda)^{-1}$ describes a strictly proper, exponentially stable transfer function [39]. Using Theorem 1 and the fact that $S \in \mathcal{L}_2$, we conclude $\zeta \in \mathcal{L}_2 \cap \mathcal{L}_\infty$, $\dot{\zeta} \in \mathcal{L}_2$, and hence $\zeta \rightarrow 0$ as $t \rightarrow \infty$. The fact that auxiliary error, ζ , converges to zero, shows the objective of achieving the desired impedance relation in equation (29).

(d) By taking the derivative of both sides of equation (30) and rearranging the terms, we have:

$$\dot{q} = \dot{q}^d - \dot{\zeta} - p[p^2 M + pB + K]^{-1} \mathcal{T}_{ext} \quad (38)$$

Using equation (37b), equation (38) can be represented in a feedback interconnection form as depicted in Fig 6(a). Here we define $\text{ENV}(\dot{q})$ as a passive operator that maps \dot{q} to \mathcal{T}_{ext} . The environment (load) is passive because the load is assumed to be a pure mass that is held by grasping. Since it is passive, we can write:

$$\langle \mathcal{T}_{ext} | \dot{q} \rangle_T \geq -\tilde{\beta} \quad (39)$$

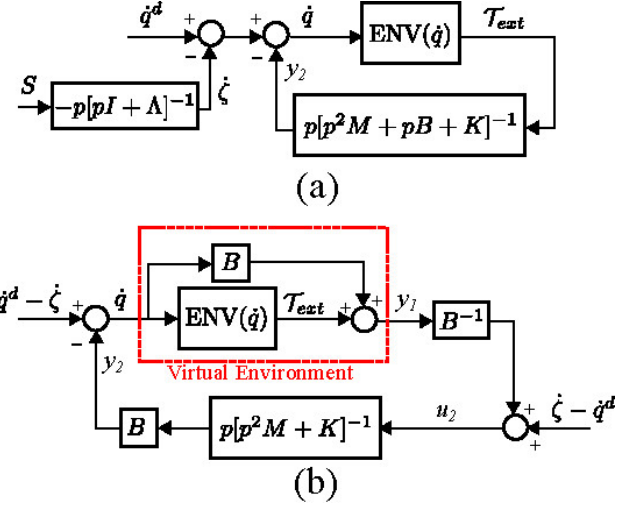


Fig. 6. (a) Feedback interconnection with one external input. (b) Transformation of interconnection to two external inputs.

It can be easily shown that the operator $\bar{H}_2 \triangleq p[p^2 M + pB + K]^{-1}$ is only passive. Therefore, this feedback loop does not reveal any information about boundedness of signals and it is inconclusive. By performing the loop transformation technique [38], [37], the equivalent interconnection can be presented as Fig 6(b). In this figure, the virtual environment operator (H_1) is composed of passive environment as represented by equation (39) and a feed forward term. So it is an ISP system with the following property:

$$\langle y_1 | \dot{q} \rangle_T \geq -\tilde{\beta} + \lambda_B \|\dot{q}\|_{2,T}^2 \quad (40)$$

where $\lambda_B > 0$ is the smallest eigenvalue of the gain matrix B . The operator $H_2 \triangleq pB[p^2 M + K]^{-1}$, which maps u_2 to y_2 , is only passive. By comparing Fig 6(b) and Fig 1, and using equation (4), we can conclude that $\epsilon_1 = \lambda_B$, $\epsilon_2 = \delta_1 = \delta_2 = 0$. Based on Lemma 1, we can write:

$$\bar{c}_2 \|y_2\|_{2,T}^2 \leq \bar{c}_3 \|\dot{q}^d - \dot{\zeta}\|_{2,T}^2 + \bar{c}_4 \|\dot{\zeta} - \dot{q}^d\|_{2,T}^2 - \bar{\beta} \quad (41)$$

where \bar{c}_i can be always chosen as positive numbers. It was shown that $\zeta \in \mathcal{L}_2$ and also using the fact that desired trajectory is bounded, we can conclude $\dot{q}^d, \dot{\zeta} \in \mathcal{L}_{2e}^n$. Therefore, the right-hand side of equation (41) is in \mathcal{L}_{2e}^n and so is the left-hand side, i.e. $y_2 \in \mathcal{L}_{2e}^n$ and bounded. Consequently, all signals inside the loop are bounded, i.e. $\dot{q}, \mathcal{T}_{ext}, y_1, u_2 \in \mathcal{L}_{2e}^n$.

In particular, $\exists \bar{\mathcal{T}}$ such that $\|\mathcal{T}_{ext}\| \leq \bar{\mathcal{T}}$. The impedance relation as a function of the auxiliary error in equation (30), can be rewritten as:

$$M\ddot{Z} + B\dot{Z} + KZ = \mathcal{T}_{ext} \quad (42)$$

where $Z = \tilde{q} - \zeta$. It can be shown that all solutions of equation (42) comply with the inequality:

$$\max(\|\dot{Z}\|_{2,T}, \|Z\|_{2,T}) \leq C^{-\kappa t} \sqrt{\|\dot{Z}_0\|^2 + \|Z_0\|^2} + \frac{C\bar{T}}{\kappa} \quad (43)$$

where C is a constant, $\kappa > 0$, and \dot{Z}_0, Z_0 are the initial conditions [43]. Because the right-hand side of equation (43) is monotonically decreasing and tends to a finite value and $\zeta \in \mathcal{L}_2$, we have $q \in \mathcal{L}_2^n$.

VII. OPTIMIZATION PROBLEM

We aim to find the impedance gains, B and K , that maximize the energy regeneration given the pre-designed references used in the impedance relation of 29. Maximizing ΔE_s in equation (26) means less amount of energy is drawn from the storage element. A value of $\Delta E_s > 0$ indicates energy regeneration and $\Delta E_s < 0$ indicates energy consumption. Considering constant impedance parameters first, we define the damping and stiffness gains as:

$$\begin{cases} B = B_c + \bar{B} \\ K = K_c + \bar{K} \end{cases} \quad (44)$$

where B_c and K_c are fixed and \bar{B} and \bar{K} are limited within an upper- and lower-bounds. The optimization is aimed to find \bar{B} and \bar{K} such that ΔE_s is maximized. Considering equation (26) and the constraints in equation (23), a static optimization problem is formulated as:

$$\max_{\bar{B}, \bar{K}} \Delta E_s = \int_0^T (\dot{q}^T \mathcal{T}^v - (\mathcal{T}^v)^T R_a \mathcal{T}^v) dt \quad (45a)$$

$$\text{subject to: } \begin{cases} \text{I} & : P_i(q_i) + r_i(q_i) = P_i(q_i) + r_i(q_i) \\ \text{II} & : \Gamma_i(q_i) - \Gamma_k(q_i) = \delta R_{ii} \quad i, \hat{i} \in \{1, \dots, N\} \\ \text{III} & : -V_s \bar{a}_R \leq \mathcal{T}^v \leq V_s \bar{a}_R \\ \text{IV} & : LB_B \leq \bar{B} \leq UB_B \\ \text{V} & : LB_K \leq \bar{K} \leq UB_K \end{cases} \quad (45b)$$

where the conditions I and II are the translational and rotational constraints, condition III is derived from equation (24) and the fact that $-1 \leq u_{ij} \leq 1$. $\bar{a}_R = \text{Vec}(a_{ij}/R_{ij}) \in \mathbb{R}^{nN}$ and $\text{Vec}(\cdot)$ represents the vectorization operator which creates a column vector by stacking a_{ij}/R_{ij} for all joints. The lower- and upper-bound for the damping and stiffness gains are indicated in conditions IV and V, respectively. These bounds determine the search area for the gains. The problem can be solved with a variety of suitable methods, such as the genetic algorithm used in the simulation example.

VIII. SIMULATION

To simulate CRM system using the proposed impedance control, two identical RRR planar robots are considered. The robots are grasping a rigid rod as shown in Fig. 7. It is assumed the actuators in the robots are DC motors and all joints are powered using an ultracapacitor as storage element. The robots' and the rod's parameters are given in Table I.

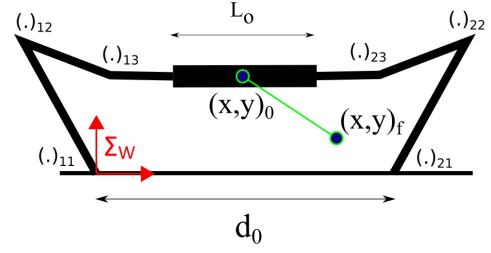


Fig. 7. Setup for two identical cooperative robots carrying a load. The world frame is attached to the base of the left robot. The distance between robots is $d_0 = 0.8$ m and robots are placed on the same level. $(\cdot)_{ij}$ represents any parameter for the j th joint of i th robot.

The motion task objective is defined as moving the load's center of mass (CM) from initial position, $(x, y)_0$, to final position, $(x, y)_f$, along a pre-designed desired trajectory. The final condition is relaxed to allow for a search of the optimal impedance gains. Accordingly, a set has been defined as:

$$IS = \{p_o(t) \mid \|p_o(t) - p_o^d(t_f)\| \leq \epsilon_f\} \quad (46)$$

where $p_o(t)$ is the position of the load's CM, $p_o^d(t_f)$ is the final desired position, $\|\cdot\|$ is the Euclidean norm, and ϵ_f is a scalar boundary. It is assumed that the motion tasks starts from the initial position, and it is accomplished whenever the final position enters the IS set. After finishing the maneuver, the load will be detached from the robots.

The desired load trajectory is based on quintic polynomial and consists of moving the load 0.4 m in the x direction, -0.4 m in the y direction, and a rotation of zero degrees in 1 s. The desired trajectories in joint space is obtained using equations 28.

The fixed inertia, damping, and stiffness impedance gains are selected as $M = \text{diag}(18)$, $B_c = \text{diag}(197.5)$, and $K_c = \text{diag}(825)$. Note that the same parameters are selected for both robots. The optimization in equation 45 is solved using genetic algorithm (GA). The optimization searches for 12 variables (one damping and one stiffness gain for each joint). The upper- and lower-bounds for the damping and stiffness gains in each joint are $-22 \leq \bar{B}_{ij} \leq 22$ and $-75 \leq \bar{K}_{ij} \leq 75$, respectively. The values and types of GA operators of this study are given in Table II.

The optimization gives the following impedance gains as

TABLE I
THE PARAMETERS FOR TWO IDENTICAL ROBOTS AND THE LOAD (ROD).

Parameter	Value	Unit
Robot:		
1st, 2nd, and 3rd arm lengths	[0.425, 0.39, 0.13]	m
1st, 2nd, and 3rd arm masses	[8.05, 2.84, 1.37]	kg
DC motor resistance	0.4	Ω
DC motor torque constant	0.07	Ω
DC motor gear ratio	50	-
Rod:		
Mass	5	kg
Length (L_0)	0.5	m

TABLE II
PARAMETERS OF GENETIC ALGORITHM.

Parameter	Value
Initial population size	50
Max. No. of generation	30
Crossover probability	0.75
Mutation rate	0.02

optimal values:

$$B_1 = \begin{bmatrix} 176.1 & 0 & 0 \\ 0 & 178.0 & 0 \\ 0 & 0 & 181.0 \end{bmatrix}, B_2 = \begin{bmatrix} 175.6 & 0 & 0 \\ 0 & 176.8 & 0 \\ 0 & 0 & 176.3 \end{bmatrix}$$

$$K_1 = \begin{bmatrix} 752.9 & 0 & 0 \\ 0 & 754.2 & 0 \\ 0 & 0 & 763.6 \end{bmatrix}, K_2 = \begin{bmatrix} 756.4 & 0 & 0 \\ 0 & 761.2 & 0 \\ 0 & 0 & 755.1 \end{bmatrix}$$

where subscripts 1 and 2 denote the matrix for the first and second robot (in Fig. 7, the robot on the left is named robot 1 and the right one is called robot 2). Figures 8 and 9 show the time histories of the reference trajectory and the actual angles for both robots. The reference trajectories are closely tracked due to the relatively high value chosen for K_c . The 2D movement is depicted in Fig. 10 and the virtual controls are shown in Fig. 11.

The power consumption in each joint is shown in Fig. 12. Positive power indicates power consumption by the joint and negative power shows energy regeneration. The energy consumption and regeneration is more pronounced in the first joint of each robot.

Figure 13 shows the Sankey diagrams for the external energy balance of equation 27. Most of the energy needed to accomplish the motion task was recovered from the potential energy difference between the initial and final positions. This is a direct consequence of maximizing energy regeneration. To study the effect of energy regeneration, we conclude the results by defining the effectiveness of energy regeneration as [1]:

$$\epsilon = 1 - \frac{\Delta E_R}{\Delta E_{NR}} \quad (47)$$

where ΔE_R and ΔE_{NR} are the system energy consumption with and without energy regeneration, respectively. ΔE_{NR} is computed by integrating the power flows in all joints, assuming any negative power is dissipated (i.e. P_{ij} ($P_{ij} \leq 0$) = 0). We have $0 \leq \epsilon \leq 1$ where $\epsilon = 0$ means energy regeneration has zero effect in reducing the energy consumption and $\epsilon = 1$ indicates that energy regeneration completely reduces energy consumption. For the condition of simulation, $\Delta E_R = 9.69 J$ and $\Delta E_{NR} = 25.84 J$ results in $\epsilon = 0.62$. This shows approximately 60% reduction in energy consumption due to energy regeneration.

A. Variable impedance parameters

The optimization in equation 45 searched for constant values of impedance gain during the motion task. It is possible to look for variable gains, i.e. $B(t)$ and $K(t)$. Variable impedance

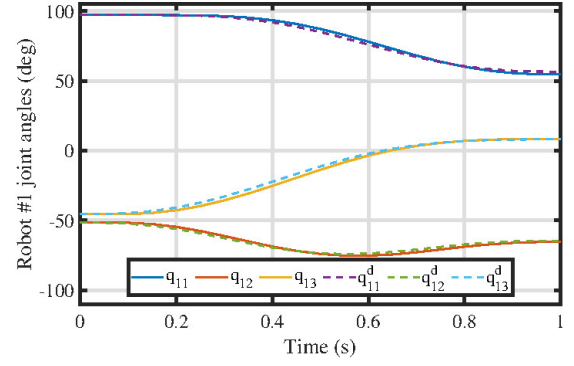


Fig. 8. The actual and desired joint angles for Robot #1.

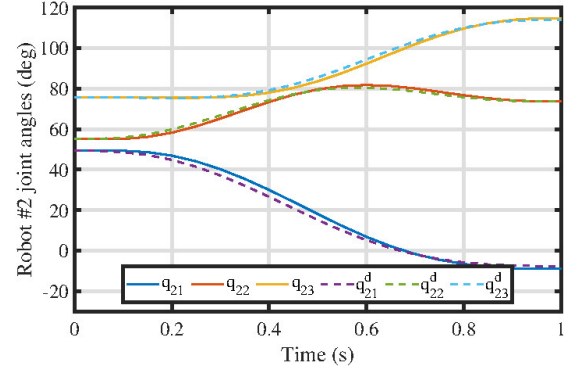


Fig. 9. The actual and desired joint angles for Robot #2.

shows better versatility when there is interaction with environment, and it has been shown to have better performance [44], [29], [45], [46], [47]. Optimal variable gains may result in further reductions in energy consumption.

If the damping and stiffness gains are time-varying matrices constrained to be positive definite, the relation between y_2 and u_2 in Fig. 6(b) can be written in the format of a linear time-varying system as:

$$\dot{\mathcal{X}}(t) = \mathfrak{A}(t)\mathcal{X}(t) + \mathfrak{B}u_2(t) \quad (48a)$$

$$y_2(t) = \mathfrak{C}(t)\mathcal{X}(t) \quad (48b)$$

where

$$\mathfrak{A}(t) = \begin{bmatrix} \mathbf{0} & \mathbf{1} \\ -M^{-1}K(t) & \mathbf{0} \end{bmatrix}, \mathfrak{B} = \begin{bmatrix} \mathbf{0} \\ M^{-1} \end{bmatrix}, \mathfrak{C}(t) = [\mathbf{0} \quad B(t)]$$

In the above matrices, $\mathbf{0} \in \mathbb{R}^{nN \times nN}$ is a null matrix and $\mathbf{1} = \text{diag}(1) \in \mathbb{R}^{nN \times nN}$ is a diagonal matrix.

Variable gains may result in the loss of passivity in the desired impedance relation [44]. However, we establish a result providing conditions to preserve passivity in the time-varying case:

Theorem 3. *The states of the system are bounded and passivity is guaranteed if the following condition is satisfied:*

$$\bar{\lambda} < 2\lambda_B^2 \quad (49)$$

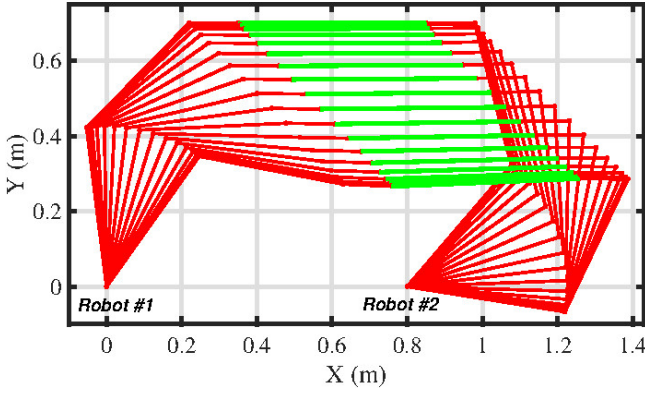


Fig. 10. Movement in 2D. Frames are captured in each 0.05 s.

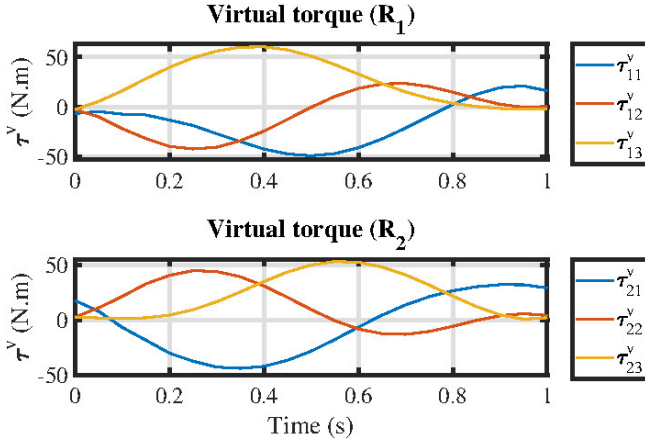


Fig. 11. Virtual torques applied to the robots.

where $\underline{\lambda}_B$ is the smallest eigenvalue of $B(t)$, $\bar{\lambda}$ is the largest eigenvalue of $\dot{P}(t) + P(t)\mathfrak{A}(t) + \mathfrak{A}^T(t)P(t)$, and $P(t) = P^T(t)$ is a positive-definite matrix defined as:

$$P(t) = \begin{bmatrix} K(t) & \mathbf{0} \\ \mathbf{0} & MB(t) \end{bmatrix} \quad (50)$$

Proof. We assume $B(t)$ and $K(t)$ are bounded, diagonal, positive definite matrices, therefore $P(t)$ is a continuous and bounded positive-definite matrix. Henceforth, to be concise, we will neglect writing the temporal argument. To study the passivity of the time varying linear system in equation (48), the following storage function and its temporal derivative can be considered [48]:

$$\mathcal{V} = \frac{1}{2} \mathcal{X}^T P \mathcal{X} \quad (51a)$$

$$\dot{\mathcal{V}} = \frac{1}{2} \mathcal{X}^T \{ \dot{P} + P\mathfrak{A} + \mathfrak{A}^T P \} \mathcal{X} + \mathcal{X}^T P \mathfrak{B} u_2 \quad (51b)$$

Integrating $\dot{\mathcal{V}}$ in the time interval $[0, T]$ gives:

$$\int_0^T \dot{\mathcal{V}}(\xi) d\xi = \mathcal{V}(T) - \mathcal{V}(0) \geq -\mathcal{V}(0) \quad (52)$$

Substituting equation (51b) in the above inequality results in the following inequality:

$$\int_0^T \left[\frac{1}{2} \mathcal{X}^T \{ \dot{P} + P\mathfrak{A} + \mathfrak{A}^T P \} \mathcal{X} + \mathcal{X}^T P \mathfrak{B} u_2 \right] d\xi \geq -\mathcal{V}(0) \quad (53)$$

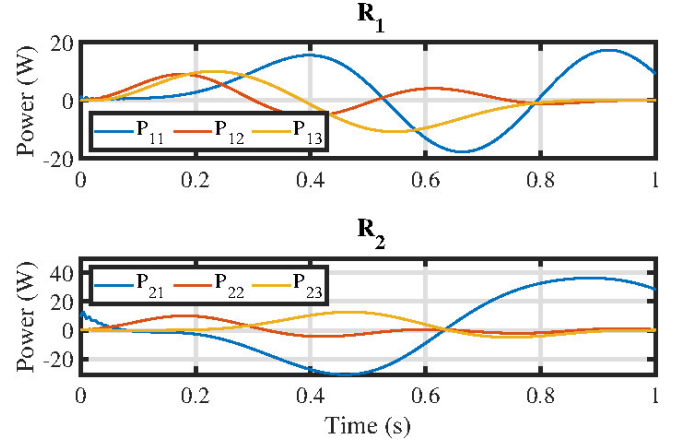


Fig. 12. Power in each joint.

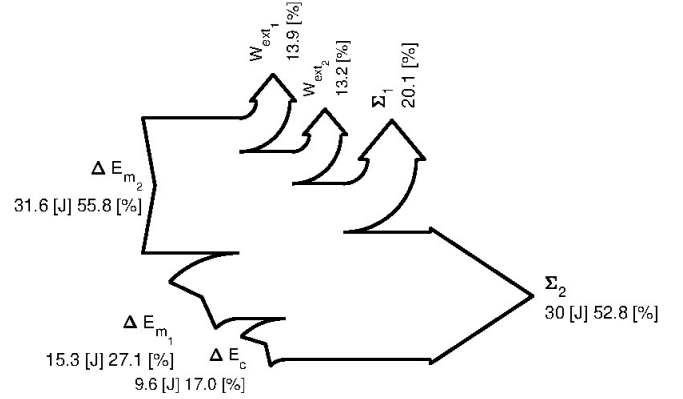


Fig. 13. Sankey diagram showing the energy balance for the CRM when following the desired trajectory.

Because $P\mathfrak{B} = \mathfrak{C}^T$, assuming $\bar{P} = \dot{P} + P\mathfrak{A} + \mathfrak{A}^T P$, we have:

$$\int_0^T \frac{1}{2} \mathcal{X}^T \bar{P} \mathcal{X} d\xi + \int_0^T y_2^T(\xi) u_2(\xi) d\xi \geq -\mathcal{V}(0) \quad (54)$$

where:

$$\bar{P} = \begin{bmatrix} \dot{K} & K - K^T B^T \\ K^T - BK & M\dot{B} \end{bmatrix} \quad (55)$$

To study the passivity of input/output in the above inequality, we study three cases of \bar{P} being negative-definite (ND), positive-definite (PD), and indefinite (ID).

1) In case of ND, the integral including \bar{P} is negative, so inequality (54) can be written as:

$$\langle y_2 | u_2 \rangle_T \geq -\mathcal{V}(0) \quad (56)$$

which proves the passivity of the system and therefore, Theorem 2 and its results are valid.

2) In the case of PD, because $\bar{P} > 0$, passivity can not be concluded directly from equation (54). In this case, we consider the following inequalities:

$$\frac{\underline{\lambda}}{2} \int_0^T \mathcal{X}^T \mathcal{X} d\xi \leq \int_0^T \frac{1}{2} \mathcal{X}^T \bar{P} \mathcal{X} d\xi \leq \frac{\bar{\lambda}}{2} \int_0^T \mathcal{X}^T \mathcal{X} d\xi \quad (57)$$

where $\underline{\lambda} > 0$ and $\bar{\lambda}$ are the smallest and biggest eigenvalues of \bar{P} , respectively. Also, in the view of output in equation (48b), we can write:

$$\underline{\lambda}_B \int_0^T \mathcal{X}^T \mathcal{X} d\xi \leq \int_0^T \mathcal{X}^T \mathcal{C}^T \mathcal{C} \mathcal{X} d\xi \leq \bar{\lambda}_B \int_0^T \mathcal{X}^T \mathcal{X} d\xi \quad (58)$$

where $\underline{\lambda}_B > 0$ and $\bar{\lambda}_B$ are the smallest and biggest eigenvalues of \mathcal{C} , respectively. From equations (57) and (58), the following inequality can be resulted:

$$\frac{\bar{\lambda}}{2} \int_0^T \mathcal{X}^T \mathcal{X} d\xi \leq \frac{\bar{\lambda}}{2\underline{\lambda}_B} \int_0^T y_2^T y_2 d\xi \quad (59)$$

Using the above inequality together with inequality (54), we have:

$$\langle y_2 | u_2 \rangle_T \geq -\mathcal{V}(0) - \frac{\bar{\lambda}}{2\underline{\lambda}_B} \|y_2\|_{2,T}^2 \quad (60)$$

From Lemma 1 and in the view of closed-loop interconnection in Fig 6, we know the lack of passivity in output of one system can be compensated by passivity in input of the other system. In other word, if $\delta_2 + \epsilon_1 > 0$, then all results in Theorem 2 are valid. Therefore, from equations (40) and (60), the passivity is guaranteed if:

$$\underline{\lambda}_B - \frac{\bar{\lambda}}{2\underline{\lambda}_B} > 0 \Rightarrow \bar{\lambda} < 2\underline{\lambda}_B^2 \quad (61)$$

3) In the case of ID, using the fact that an indefinite matrix has at least one positive eigenvalue and at least one negative eigenvalue, we can assume that $\bar{\lambda} > 0$ and all results for PD case are valid for ID case.

In conclusion, the gain matrices can vary as long as inequality (61) is satisfied. If the change, i.e. sign of K and B , leads to a ND value for \bar{P} , inequality (61) is automatically satisfied, and the passivity is preserved. If the change leads to PD value for \bar{P} and inequality (61) is effective, system stays passive. If none of above happens and change leads to an ID \bar{P} , having inequality (61) would be enough for the passivity. Note that the variation of damping matrix does not affect the passivity of H_1 in the interconnection of Fig. 6(b). \square

IX. CONCLUDING REMARKS AND FUTURE WORKS

In this research, a framework is established for controlling cooperative robots and executing the motion task of moving a load along a desired trajectory. A comprehensive model of an augmented dynamics of the robot, JMs and the motors, provides the opportunity to introduce a new control scheme for semi-active joints called virtual control strategy (SVC). Based on SVC, any suitable control approach can be utilized to control the motion task in CRM. Here we used the concept of impedance control to devise the control scheme. The controller was studied and developed for two cases; constant damping and stiffness gains in the impedance relation; and variable gains. For both cases, the input/output passivity tool was used to analysis the stability.

Moreover, an optimization was introduced to obtain an energy-oriented impedance control. The optimization finds the best impedance gains such that the energy extraction from the

power source is minimized. Using a simulation example, it was shown that energy regeneration can occur during the motion task, and it has huge effect in terms of energy saving.

The lab experiment of this research is left as the future work. Also, another possible future work is to find an energy-optimal path for moving the load from point to point, which requires forming an optimization to find the optimal trajectory.

APPENDIX A

EXTERNAL ENERGY BALANCE IN CRM

We start by obtaining Joule losses in terms of the desired control. The Joule losses due to resistance in motor of $ijth$ semi-active joint is:

$$L_{R_{ij}} = R_{ij} I_{ij}^2 \quad (62)$$

Substituting current and u_{ij} from equations (14) and (24), respectively, and after some manipulation and simplification, we get:

$$L_{R_{ij}} = \frac{R_{ij}}{a_{ij}^2} (\tau_{ij}^d)^2 + \frac{a_{ij}^2 \dot{q}_{ij}^2}{R_{ij}} - 2\tau_{ij}^d \dot{q}_{ij} \quad (63)$$

Equation (15) expresses the relation between τ_{ij} and τ_{ij}^d . Multiplying both sides of this equation by \dot{q}_{ij} yields:

$$\tau_{ij} \dot{q}_{ij} = -m_{ij} \bar{n}_{ij}^2 \ddot{q}_{ij} \dot{q}_{ij} - (b_{ij} \bar{n}_{ij}^2 + \frac{a_{ij}^2}{R_{ij}}) \dot{q}_{ij}^2 + \tau_{ij}^d \dot{q}_{ij} \quad (64)$$

The kinetic energy of the actuator is expressed as $K_{ij} = \frac{1}{2} I_{ij} \bar{n}_{ij}^2 \dot{q}_{ij}^2$. So equation (64) can be simplified as:

$$\tau_{ij} \dot{q}_{ij} = -\frac{dK_{ij}}{dt} - (b_{ij} \bar{n}_{ij}^2 + \frac{a_{ij}^2}{R_{ij}}) \dot{q}_{ij}^2 + \tau_{ij}^d \dot{q}_{ij} \quad (65)$$

Replacing $a_{ij}^2 \dot{q}_{ij} / R_{ij}$ from equation (64) and rearranging the result and taking the integral from t_1 to t_2 of both sides of obtained equation gives:

$$\int_{t_1}^{t_2} (\tau_{ij}^d \dot{q}_{ij} - \frac{R_{ij}}{a_{ij}^2} (\tau_{ij}^d)^2) dt = \int_{t_1}^{t_2} (-\frac{dK_{ij}}{dt} - \tau_{ij} \dot{q}_{ij} - L_{R_{ij}} - b_{ij} \bar{n}_{ij}^2 \dot{q}_{ij}^2) dt \quad (66)$$

On the other hand, using ΔE_c from equation (26), we can write:

$$\Delta E_c = \sum_{i=1}^N \sum_{j=1}^n \Delta E_{c_{ij}} \quad (67)$$

where:

$$\Delta E_{c_{ij}} = \int_{t_1}^{t_2} (\tau_{ij}^d \dot{q}_{ij} - \frac{R_{ij}}{a_{ij}^2} (\tau_{ij}^d)^2) dt \quad (68)$$

Using equations (66) and (68), it can be concluded:

$$\Delta E_{c_{ij}} = \int_{t_1}^{t_2} (-\frac{dK_{ij}}{dt} - \tau_{ij} \dot{q}_{ij} - L_{R_{ij}} - b_{ij} \bar{n}_{ij}^2 \dot{q}_{ij}^2) dt \quad (69)$$

To derive equation (27), we start by writing the overall energy balance for CRM:

$$\int_{t_1}^{t_2} \dot{q}^T \mathcal{T} dt + \int_{t_1}^{t_2} \dot{q}^T \mathcal{T}_{ext} dt = \Delta E_m^o + \Sigma_m^o \quad (70)$$

where the first term on the left-hand side is the work done by the semi-active joints, the second term is the work done by the external forces and moments (W_{ext}), ΔE_m° is the total change in mechanical energy, and Σ_m° is the dissipated mechanical energy in the system. Also \mathcal{T} is defined as the vector of all applied forces/moments and $\mathcal{T}_{ext} = J^T(q)f$ is the vector of external forces/moments, i.e. the forces/moments applied by the load.

If we write equation (66) for all joints in CRM and substitute in equation (70), results:

$$W_{ext} = \Delta E_c + \Delta E_m^{Tot} + \Sigma_m^{Tot} + \Sigma_e \quad (71)$$

where

$$\begin{aligned} \Delta E_m^{Tot} &= \Delta E_m^\circ + \sum_{i=1}^N \sum_{j=1}^n \Delta K_{ij} \\ \Sigma_m^{Tot} &= \Sigma_m^\circ + \sum_{i=1}^N \sum_{j=1}^n \int_{t_1}^{t_2} b_{ij} \bar{n}_{ij}^2 \dot{q}_{ij}^2 dt \\ \Sigma_e &= \sum_{i=1}^N \sum_{j=1}^n \int_{t_1}^{t_2} L_{R_{ij}} dt \end{aligned} \quad (72)$$

ACKNOWLEDGMENT

The authors would like to thank the National Science Foundation for funding this work (NSF grant #1536035).

REFERENCES

- [1] P. Khalaf and H. Richter, "Trajectory optimization of robots with regenerative drive systems: Numerical and experimental results," *IEEE Transactions on Robotics*, vol. 36, no. 2, pp. 501–516, 2019.
- [2] H. Richter, "A framework for control of robots with energy regeneration," *Journal of Dynamic Systems, Measurement, and Control*, vol. 137, no. 9, 2015.
- [3] A. Ghorbanpour and H. Richter, "Control with optimal energy regeneration in robot manipulators driven by brushless dc motors," in *ASME 2018 Dynamic Systems and Control Conference*. American Society of Mechanical Engineers Digital Collection, 2018.
- [4] P. Khalaf and H. Richter, "Parametric optimization of stored energy in robots with regenerative drive systems," in *Advanced Intelligent Mechatronics (AIM), 2016 IEEE International Conference on*. IEEE, 2016, pp. 1424–1429.
- [5] T. Shimizu and C. Underwood, "Super-capacitor energy storage for micro-satellites: Feasibility and potential mission applications," *Acta Astronautica*, vol. 85, pp. 138–154, 2013.
- [6] P. Khalaf, H. Warner, E. Hardin, H. Richter, and D. Simon, "Development and experimental validation of an energy regenerative prosthetic knee controller and prototype," in *ASME 2018 Dynamic Systems and Control Conference*. American Society of Mechanical Engineers Digital Collection, 2018.
- [7] H. Richter, "Control for optimal energy regeneration from autorotation in uavs," in *2020 American Control Conference (ACC)*. IEEE, 2020, pp. 5108–5113.
- [8] X. He, H. Liu, S. He, B. Hu, and G. Xiao, "Research on the energy efficiency of energy regeneration systems for a battery-powered hydrostatic vehicle," *Energy*, vol. 178, pp. 400–418, 2019.
- [9] P. Boscarol and D. Richiedei, "Trajectory design for energy savings in redundant robotic cells," *Robotics*, vol. 8, no. 1, p. 15, 2019.
- [10] P. Khalaf and H. Richter, "On global, closed-form solutions to parametric optimization problems for robots with energy regeneration," *Journal of Dynamic Systems, Measurement, and Control*, vol. 140, no. 3, 2018.
- [11] H. Richter and D. Selvaraj, "Impedance control with energy regeneration in advanced exercise machines," in *American Control Conference (ACC), 2015*. IEEE, 2015, pp. 5890–5895.
- [12] H. Warner, D. Simon, and H. Richter, "Design optimization and control of a crank-slider actuator for a lower-limb prosthesis with energy regeneration," in *Advanced Intelligent Mechatronics (AIM), 2016 IEEE International Conference on*. IEEE, 2016, pp. 1430–1435.
- [13] G. Carabin, E. Wehrle, and R. Vidoni, "A review on energy-saving optimization methods for robotic and automatic systems," *Robotics*, vol. 6, no. 4, p. 39, 2017.
- [14] H. Richter, J. W. Connolly, and D. L. Simon, "Optimal control and energy management for hybrid gas-electric propulsion," *Journal of Engineering for Gas Turbines and Power*, vol. 142, no. 9, 2020.
- [15] J. Joy and S. Ushakumari, "Regenerative braking mode operation of a three-phase h-bridge inverter fed pmbldc motor generator drive in an electric bike," *Electric Power Components and Systems*, pp. 1–19, 2018.
- [16] A. Ivoilov, V. Trubin, V. Zhmud, and L. Dimitrov, "The power consumption decreasing of the two-wheeled balancing robot," in *2018 International Multi-Conference on Industrial Engineering and Modern Technologies (FarEastCon)*. IEEE, 2018, pp. 1–8.
- [17] G. Khademi, H. Mohammadi, H. Richter, and D. Simon, "Optimal mixed tracking/impedance control with application to transfemoral prostheses with energy regeneration," *IEEE Transactions on Biomedical Engineering*, 2017.
- [18] A. Koivo and M. Unseren, "Modeling closed chain motion of two manipulators holding a rigid object," *Mechanism and machine theory*, vol. 25, no. 4, pp. 427–438, 1990.
- [19] P. Chiacchio, S. Chiaverini, and B. Siciliano, "Cooperative control schemes for multiple robot manipulator systems," in *ICRA, 1992*, pp. 2218–2223.
- [20] I. D. Walker, R. A. Freeman, and S. I. Marcus, "Analysis of motion and internal loading of objects grasped by multiple cooperating manipulators," *The International journal of robotics research*, vol. 10, no. 4, pp. 396–409, 1991.
- [21] J.-H. Jean and L.-C. Fu, "An adaptive control scheme for coordinated multimanipulator systems," *IEEE Transactions on Robotics and Automation*, vol. 9, no. 2, pp. 226–231, 1993.
- [22] S. Erhart and S. Hirche, "Internal force analysis and load distribution for cooperative multi-robot manipulation," *IEEE Transactions on Robotics*, vol. 31, no. 5, pp. 1238–1243, 2015.
- [23] A. Vergnano, C. Thorstensson, B. Lennartson, P. Falkman, M. Pellicciari, F. Leali, and S. Biller, "Modeling and optimization of energy consumption in cooperative multi-robot systems," *IEEE Transactions on Automation Science and Engineering*, vol. 9, no. 2, pp. 423–428, 2012.
- [24] H. Kawasaki, S. Ueki, and S. Ito, "Decentralized adaptive coordinated control of multiple robot arms without using a force sensor," *Automatica*, vol. 42, no. 3, pp. 481–488, 2006.
- [25] R. Bonitz and T. C. Hsia, "Internal force-based impedance control for cooperating manipulators," *IEEE Transactions on Robotics and Automation*, vol. 12, no. 1, pp. 78–89, 1996.
- [26] F. Caccavale, P. Chiacchio, A. Marino, and L. Villani, "Six-dof impedance control of dual-arm cooperative manipulators," *IEEE/ASME Transactions On Mechatronics*, vol. 13, no. 5, pp. 576–586, 2008.
- [27] J. Szewczyk, F. Plumet, and P. Bidaud, "Planning and controlling cooperating robots through distributed impedance," *Journal of Robotic Systems*, vol. 19, no. 6, pp. 283–297, 2002.
- [28] M. Shimizu, "Nonlinear impedance control to maintain robot position within specified ranges," in *2012 Proceedings of SICE Annual Conference (SICE)*. IEEE, 2012, pp. 1287–1292.
- [29] J. He, M. Luo, and Q. Zhang, "Dual impedance control with variable object stiffness for the dual-arm cooperative manipulators," in *2016 Asia-Pacific Conference on Intelligent Robot Systems (ACIRS)*. IEEE, 2016, pp. 102–108.
- [30] D. Heck, D. Kostić, A. Denasi, and H. Nijmeijer, "Internal and external force-based impedance control for cooperative manipulation," in *2013 European Control Conference (ECC)*. IEEE, 2013, pp. 2299–2304.
- [31] S. Schneider and R. H. Cannon, "Object impedance control for cooperative manipulation: Theory and experimental results," in *1989 IEEE International Conference on Robotics and Automation*. IEEE Computer Society, 1989, pp. 1076–1077.
- [32] M. Li, K. Li, P. Wang, Y. Liu, F. Zha, and W. Guo, "Indirect adaptive impedance control for dual-arm cooperative manipulation," in *2017 2nd International Conference on Advanced Robotics and Mechatronics (ICARM)*. IEEE, 2017, pp. 650–655.
- [33] Y. Ren, Y. Zhou, Y. Liu, M. Jin, and H. Liu, "Adaptive object impedance control of dual-arm cooperative humanoid manipulators," in *Proceeding of the 11th World Congress on Intelligent Control and Automation*. IEEE, 2014, pp. 3333–3339.
- [34] F. Caccavale and L. Villani, "An impedance control strategy for cooperative manipulation," in *2001 IEEE/ASME International Conference on*

- Advanced Intelligent Mechatronics. Proceedings (Cat. No. 01TH8556)*, vol. 1. IEEE, 2001, pp. 343–348.
- [35] S. Erhart, D. Sieber, and S. Hirche, “An impedance-based control architecture for multi-robot cooperative dual-arm mobile manipulation,” in *2013 IEEE/RSJ International Conference on Intelligent Robots and Systems*. IEEE, 2013, pp. 315–322.
- [36] A. Stolfi, P. Gasbarri, and M. Sabatini, “A combined impedance-pd approach for controlling a dual-arm space manipulator in the capture of a non-cooperative target,” *Acta Astronautica*, vol. 139, pp. 243–253, 2017.
- [37] A. J. Van der Schaft and A. Van Der Schaft, *L2-gain and passivity techniques in nonlinear control*. Springer, 2000, vol. 2.
- [38] M. Vidyasagar, *Nonlinear systems analysis*. SIAM, 2002.
- [39] R. Ortega, J. A. L. Perez, P. J. Nicklasson, and H. J. Sira-Ramirez, *Passivity-based control of Euler-Lagrange systems: mechanical, electrical and electromechanical applications*. Springer Science & Business Media, 2013.
- [40] B. Brogliato, R. Lozano, B. Maschke, and O. Egeland, *Dissipative Systems Analysis and Control: Theory and Applications*, ser. Communications and Control Engineering. Springer International Publishing, 2019. [Online]. Available: <https://books.google.com/books?id=-ZqgDwAAQBAJ>
- [41] R. Kelly, R. Carelli, M. Amestegui, and R. Ortega, “On adaptive impedance control of robot manipulators,” in *1989 IEEE International Conference on Robotics and Automation*. IEEE Computer Society, 1989, pp. 572–573.
- [42] M. W. Spong, S. Hutchinson, M. Vidyasagar *et al.*, *Robot modeling and control*, 2006.
- [43] M. Vukobratović, “How to control robots interacting with dynamic environment,” *Journal of Intelligent and Robotic Systems*, vol. 19, no. 2, pp. 119–152, 1997.
- [44] F. Ferraguti, C. Secchi, and C. Fantuzzi, “A tank-based approach to impedance control with variable stiffness,” in *2013 IEEE international conference on robotics and automation*. IEEE, 2013, pp. 4948–4953.
- [45] M. Zheng, T. Yuan, and T. Huang, “Time-varying impedance control of port hamiltonian system with a new energy-storing tank,” *Complexity*, vol. 2018, 2018.
- [46] Y. Kishi, Z. W. Luo, F. Asano, and S. Hosoe, “Passive impedance control with time-varying impedance center,” in *Proceedings 2003 IEEE International Symposium on Computational Intelligence in Robotics and Automation. Computational Intelligence in Robotics and Automation for the New Millennium (Cat. No. 03EX694)*, vol. 3. IEEE, 2003, pp. 1207–1212.
- [47] K. Kronander and A. Billard, “Stability considerations for variable impedance control,” *IEEE Transactions on Robotics*, vol. 32, no. 5, pp. 1298–1305, 2016.
- [48] J. R. Forbes and C. J. Damaren, “Passive linear time-varying systems: State-space realizations, stability in feedback, and controller synthesis,” in *Proceedings of the 2010 American Control Conference*. IEEE, 2010, pp. 1097–1104.